Available online at www.sciencedirect.com
SCIENCE DIRECT®
Physics Letters A 336 (2005) 97–105
PHYSICS LETTERS A
www.elsevier.com/locate/pla

Low frequency vertical geometric anti-spring vibration isolators

E.J. Chin *, K.T. Lee, J. Winterflood, L. Ju, D.G. Blair

School of Physics, The University of Western Australia, Perth 6907, Australia

Received 17 December 2004; received in revised form 7 January 2005; accepted 7 January 2005

Communicated by P.R. Holland

Abstract

Euler spring vibration isolators can be significantly improved by implementing anti-spring techniques. Here we report geometric spring coefficient reduction techniques which allow an order of magnitude improvement in the effective spring coefficient, achieving a resonant frequency of 0.3 Hz. In this Letter we analyse the various effects which determine the behaviour and stability of low frequency Euler stages.

PACS: 04.80.Nn; 07.10.Fq

Keywords: Gravitational wave detectors; Vibration isolators; Euler elastic buckling

1. Introduction

Vibration isolation systems have been greatly improved to meet stringent demands for successful gravitational wave detectors. Their purpose is to attenuate seismic vibrations from the ground to levels below the internal thermal noise of the test masses. This is achieved by using a system of cascaded mass-spring harmonic oscillators in which each mass is suspended with soft restoring forces. The level of isolation improves as the characteristic frequencies are reduced, and as more stages are cascaded.

To attenuate vertical seismic motion, vibrational energy between the suspension point and the test mass has to be momentarily stored and then recovered with low loss from a spring or a similar element. Many new techniques have been developed. The gravity group at the University of Western Australia (UWA) first introduced the use of curved cantilever springs in 1990 for gravitational wave applications [1,2]. These are now widely used for vertical isolation. The super-attenuators of VIRGO [3,4] have sets of triangular cantilever springs. GEO600 uses similar blades [5]. Both VIRGO and TAMA [6,7], use blade structures combined with anti-spring

* Corresponding author. Mr. Eu-Jeen Chin, School of Physics, The University of Western Australia, 35 Stirling Hwy, Crawley, WA 6907, Australia.
E-mail address: ejc@physics.uwa.edu.au (E.J. Chin).

0375-9601/$ – see front matter
doi:10.1016/j.physleta.2005.01.013

methods to lower the resonant frequency [8]. LIGO is developing active vibration isolation [9] in which very sensitive seismometers are used to suppress noise by actuation on a relatively stiff isolation structure. In 2001 the UWA gravity group introduced Euler springs for vibration isolation [10]. These have significantly improved performance compared with blades due to their low mass and high internal mode frequencies. It is planned that together with a LaCoste linkage [11], three stages of Euler spring isolators will be used for the vertical vibration isolation system for the Australian International Gravitational Observatory (AIGO).

In this Letter we show that by implementing anti-spring techniques the resonant frequency of Euler springs can be significantly reduced. First we give an introduction to Euler springs including results from previous studies. Then we analyse a configuration in which an anti-spring is included in the suspension structure. In Section 4 predictions are compared with experimental results.

2. Euler buckling and non-linearities

An Euler spring is a column of spring material that has been compressed elastically beyond its buckling load. A major advantage in using this type of spring is that it stores negligible static energy below its working range thereby minimising both the stored elastic energy density and the spring mass required to support the suspended test mass [10]. As a result, the resonant frequency of the internal modes of the spring elements is increased, thus broadening the isolation bandwidth. An ideal Euler spring by itself produces an almost constant spring coefficient over a large working range. Also, the spring is small in size compared to its equivalent cantilever spring allowing for the construction of more compact 3D vibration isolators.

Preliminary analysis [12] and testing reveal that the performance of Euler springs can be strongly manipulated by their constraining mechanism. Pivoting rotational lever arms (see Fig. 3) are used to constrain the loading direction and displacement allowing them to be compressed in the longitudinal direction. The spring deformation may be either towards or away from the pivot point. These two alternatives yield quite different force–displacement curves which differ significantly from the ideal behaviour discussed above. It has been shown that an Euler spring buckling towards the pivot has non-linear and much lower effective spring coefficients than buckling away from the pivot [10–13]. The force–displacement curves can have a turning point leading to regions of instability. When the spring bend away from the pivot higher spring coefficients are obtained. In the case of an equally balanced pair of springs buckling towards and away from the pivot (see Fig. 3), an almost constant spring coefficient is observed. Springs in pairs are usually necessary to permit spring coefficient reduction over a useful operating range.

Another non-linearity arises when the launching angle of a spring is non-ideal. The launching angle is defined as the angle at which the Euler springs are clamped (see diagrams in Fig. 1). This value, measured from the vertical, is the effective clamping angle of a set of springs in a single ideal Euler stage. If the launching angle at both ends of a pair of springs are equal and deflected in the same rotational direction (so

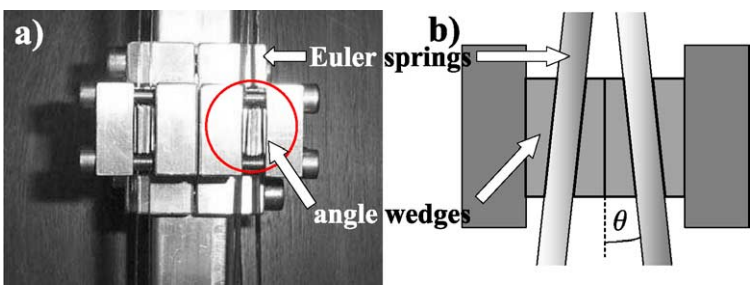

Fig. 1. (a) Photograph of the Euler spring clamps in the vertical isolation stage, (b) diagram of the configuration of a pair of springs using wedges to achieve the desired launch angle θ.

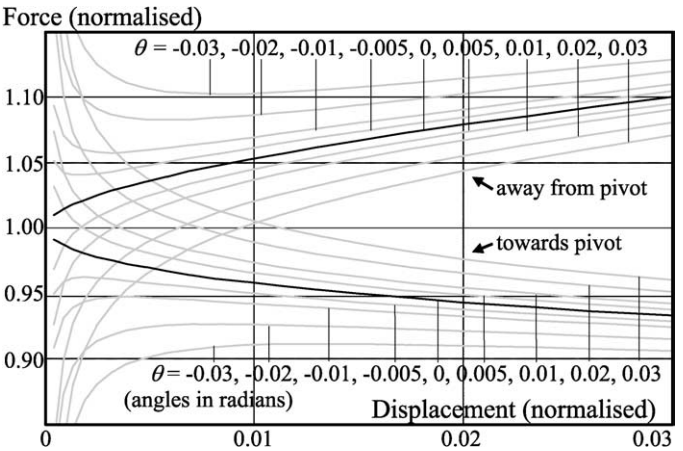

Fig. 2. The force–displacement curves of the Euler stage (adapted from [12]). Note the non-linear behaviour of the curves as the launching angle θ is varied over a range from -0.03 to $+0.03$ radians. The desired working range is located in regions of constant spring coefficients. By varying the amount of launching angle the shape of the force–displacement curve can be manipulated and thus improve the performance of the Euler stage.

as to produce an 'S' bend shape on buckling), the non-linear effects cancel out. In other words, the launching angle for this pair of springs is zero. In Ref. [12] a mathematical analysis of the performance of the Euler stage was derived. This involved using parametric equations which describe the shape of the spring, called an *elastica*. The analysis predicted how differing launching angles in the Euler stage influence the behaviour of the system. A set of force–displacement curves was obtained, reproduced here in Fig. 2. The graph is labelled with normalised values, with respect to the critical force and spring length. In the plot, it assumes that the radius of the lever arm (the distance from the pivot to the top spring clamp) is equal to length of the spring. The upper part of the graph corresponds to the spring bending away from the pivot while the lower part corresponds to bending towards the pivot. The two dark lines indicate the zero launching angle case while the shaded lines are achieved by fine adjustments in the launch angles. The symbol θ represents the effective launching angle (in radians) that is applied to the springs, predisposing it to buckle in one sideways direction rather than the other. Negative values represent angles opposing the spring buckling direction. If the proportion of springs bending in each direction is varied any intermediate curve can be obtained. Notice the high sensitivity of the spring constant to the value of θ.

3. Spring coefficient reduction

One method of frequency reduction is through the use of an anti-spring with a negative spring coefficient (i.e., producing an anti-restoring or destabilising force). When combined with the appropriate positive spring coefficient, a very low spring coefficient can be achieved. The VIRGO group incorporated anti-springs by using cantilevers fitted with repelling magnets [3]. Another spring coefficient reduction technique was demonstrated using a torsion-crank suspension [14]. Similar systems presented by Bertolini [15] and Cella [16] were termed 'geometric anti-springs'.

The turning points in Fig. 2 represent intrinsic anti-spring behaviour, but these offer a very low dynamic range. Fig. 2 shows that the spring coefficient is approximately constant for relative displacements greater than about 1.5%. We go on now to present a configuration that implements geometric variation into the Euler stage to reduce the spring coefficient further [10]. Having the mass suspension points located above the top Euler spring clamps provides the geometric anti-spring effect as shown in Fig. 3. The value h is defined as the distance between the top of the clamped Euler spring and the bottom of the wire holder which is the suspension point. This h component is essentially an inverse pendulum.

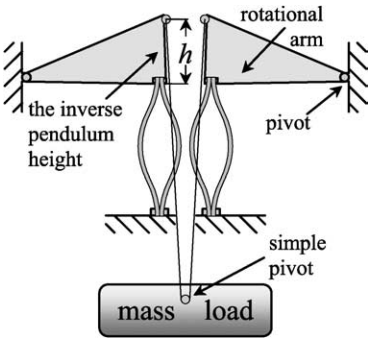

Fig. 3. Diagram of the Euler system consisting of two pairs of Euler springs and an inverse pendulum of height h in the rotational arms [10].

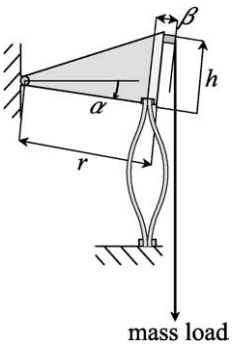

Fig. 4. Diagram showing the modelling parameters.

3.1. Mathematical model

The model presented here considers how the stored energy varies with the height of the mass load using the parameters defined in Fig. 4 [17]. There are two principle energy storage elements. The first is the compression of the Euler springs. The second is unavoidable and significant: an effective spring due to the various flexures and the suspension wires that bend as the rotational arm moves. The force of the latter varies with angle α and some coefficient K_w and is represented by the first term in Eq. (1). The compression force from the Euler spring can be considered as the sum of the critical buckling force F_{cr} and a force which varies as compression distance with an approximately constant coefficient of $F_{\mathrm{cr}}/2l$, where l is its unbuckled length. We then obtain the following energy equation:

$$\mathrm{Energy}(\alpha) = \frac{1}{2}K_w\alpha^2 + \frac{1}{2}\frac{F_{\mathrm{cr}}}{2l}r^2\big(\sin(\alpha)\big)^2 + F_{\mathrm{cr}}r\sin(\alpha). \quad (1)$$

In our case the lever radius r is 64 mm and the springs are assumed to have a total critical load of 380 N with an unbuckled length l of 134 mm. The term K_w is typically dominated by the bending stiffness of the suspension wires (as they have to be reasonably strong). As shown in Ref. [12], K_w contributes approximately an additional 6% of the Euler spring coefficient at this loading. The vertical displacement y at the suspension point is derived through simple geometry. For inverse pendulum height h:

$$y(\alpha) = h - \sqrt{r^2+h^2}\sin\big(\arctan(h/r) - \alpha\big) - \beta\sin(\alpha). \quad (2)$$

The last term in Eq. (2) is due to an extension of the wire holding mechanism, where β is the offset distance in the plane of the rotational arm between the point at which the wire suspends the load and the apex of the Euler spring (see Fig. 4). Our experimental value for β is 10 mm. From Eqs. (1) and (2) we can obtain:

$$F_y = \frac{\partial_\alpha \mathrm{Energy}(\alpha)}{\partial_\alpha y(\alpha)}. \quad (3)$$

The wire thickness contributes to an addition of stiffness to the system as well as the undesired lowering of the suspension point. A new point of suspension is situated lower than the height of the wire holder due to the bending of the wire [18].

The resulting force–displacement curve is shown in Fig. 5 illustrating the large effects the value h has on the vertical system. Here the x-axis is the vertical displacement at the suspension point as a function of α. The force is normalised to the critical force which is the force needed to start buckling the springs. The displacement is normalised to the length of the Euler springs.

In this particular model the parameters are chosen as close as possible to the real experimental apparatus. The curves on the graph show the effect of incorporating various amounts of inverse pendulum height into the rotational arms. It shows that provided the launching angles are well defined and set, and the correct amount of geometric spring coefficient reduction is added, it is theoretically possible to achieve an arbi-

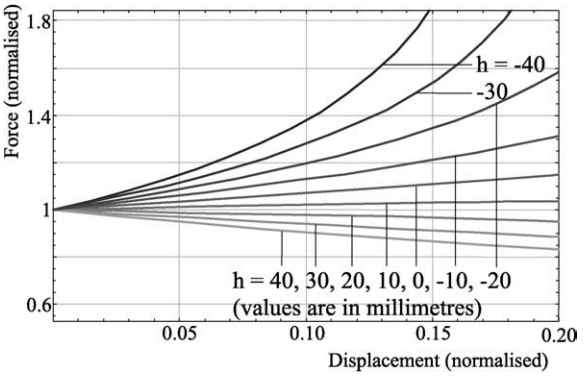

Fig. 5. The force–displacement curves shown here with varying h values suggests that low resonant frequencies can theoretically be achieved by this spring coefficient reduction technique. In reality, the performance of the springs only benefit when operating at small spring buckling deflections (to about 3% of their unbuckled length).

trarily low resonant frequency. In practice, the system becomes inoperable when the Q-factor approaches unity. At this point, inelastic and hysteretic effects begin to dominate. For the structural damping expected here the Q-factor decreases proportional to the frequency squared.

4. The performance of the Euler stage

For experimental purposes the Euler stage was supported by a platform attached to a square central tube. The Euler springs were clamped to the lower end of the central tube as well as to the rotational arms as shown in Fig. 6. Suspension wires pass through the tube to a suspended mass below the Euler stage. The adjustment of the inverse pendulum height h was achieved by moving the suspension points in the vertical direction along slotted plates. A more detailed description of the construction of the Euler stage was previously published in Section 7 of Ref. [10]. Although the publication was based on an older design, the main concepts are still used and can be sought for an easier understanding of the construction process.

The Euler spring material used for initial testing was AISI C1095 tool steel in the form of a feeler gauge strip. The reason for the choice of the material was its easy availability in different thicknesses. A constant Euler spring length of 134 mm with the thickness of 0.5 mm was used throughout experimentation for easy comparison between results.

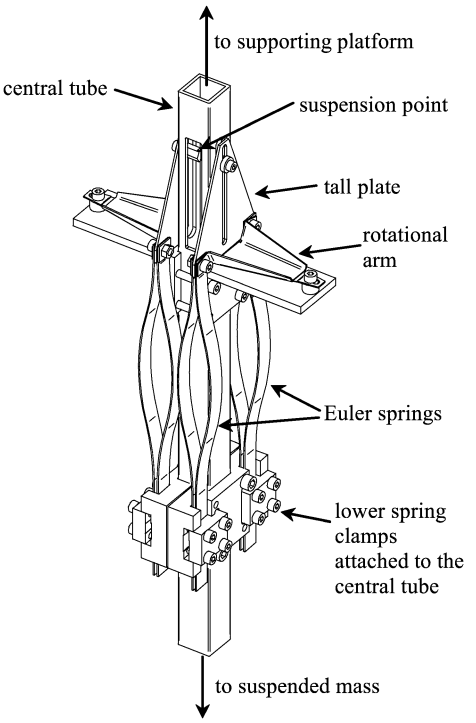

Fig. 6. An assembly drawing of the vertical Euler stage showing the tall geometric inverse pendulum plates. Eight Euler springs are used in the stage and are paired together so four would deflect one way and the other four in the opposite direction [17].

Shadow sensors were used for measuring vertical displacement in the Euler stage. A geophone was also used to verify the resonant frequency peaks. Vertical displacement was measured at the rotational arm. Launching angle adjustments were provided by different angled aluminium wedges that were clamped together with the Euler springs (as shown in Fig. 1). A signal analyser was used to obtain transfer functions across the frequency spectrum.

Transfer functions were obtained by suspending the supporting platform, which was attached to the top end of the central tube, by coil springs. A loud speaker voice coil assembly was used to excite the platform. A geophone was placed on top of the platform to measure the input motion while another was placed centrally on the test mass to measure the output response.

4.1. Results

The first results presented here are for springs with zero launching angle. Fig. 7 shows a typical set of

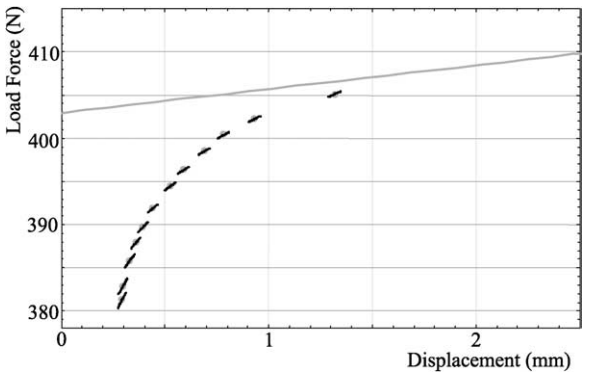

Fig. 7. A force vs. displacement graph with an h value of 22 mm. Note the extreme curvature of the data points approaching the theoretical curve in the ideal case.

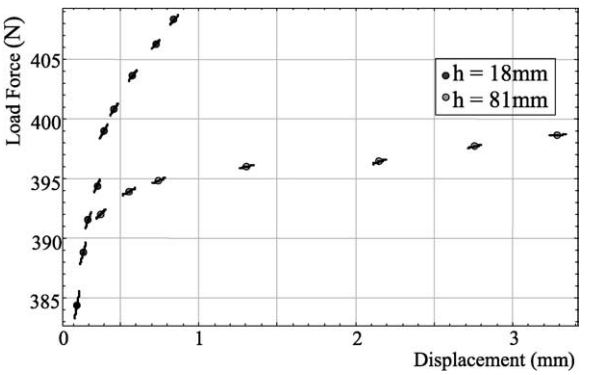

Fig. 8. A plot showing strong inverse pendulum tuning of the Euler stage. With $h = 81$ mm the slope is reduced substantially compared with the system with $h = 18$ mm.

data. It is a force–displacement plot with an h value of 22 mm and a wire diameter of 2 mm. The resonant frequency was recorded simultaneously, determining the gradient lines for each data point. The initial displacement offset of the theoretical straight line is determined using a first order approximation equation describing *elastica* [12]:

$$y = 2l - 2\sqrt{l^2 - b^2\pi^2}. \tag{4}$$

Here y is the vertical change of length from the unbuckled springs, l is the length of the Euler springs and b is half the horizontal buckling displacement of the springs. The contribution of the stiffness of the rotational arm at the flexure point is small; having a spring coefficient of 800 N/m and only becomes significant at very low resonant frequencies.

The curvature in the experimental data is immediately apparent when compared with the theoretical straight line. This corresponds with a state of positive θ shown in Fig. 2. The critical Euler buckling force was determined experimentally. Its value, 403 N (41 kg), was constant and consistent for all the measurements made (further plots are not shown in this publication).

Fig. 8 compares two h values: 18 mm and 81 mm, using 1 mm diameter suspension wire. It is seen that the inverse pendulum has significant effects on the spring coefficient of the system. While Fig. 8 shows the expected qualitative behaviour, the magnitude of the anti-spring is weaker than expected. It appears that the system is sensitive to imperfections in the clamping mechanism, uneven spring lengths and creep. The inverse pendulum height of 81 mm achieved a resonant frequency of 0.67 Hz corresponding to a spring coefficient of 800 N/m. Comparing this with a spring coefficient of 8000 N/m for $h = 18$ mm, we observe a factor of ten improvement.

Fig. 9 shows the improvement in the resonant frequency as the wire diameter is changed. Here the resonant frequency is plotted against the mass load. There is a distinct gap between the data sets for 1 mm and 2 mm wires. The undesirable non-constant gradients of force–displacement plots seen earlier are also noticeable as a dependence of resonant frequency on displacement. The displacement range of the Euler spring restricts the mass load range.

Next we present experimental results involving the implementation of launching angle adjustment together with different values of the inverse pendulum height. The continuous theoretical lines in Fig. 10 and Fig. 11 were generated using numerical routines developed in Ref. [12]. The theoretical curves displayed are made to best fit the experimental data. The horizontal and vertical axes are normalised by the length of the springs (134 mm) and the critical force of the system, respectively. The routines have essentially two parameters to optimise for best fit: the adjustments of the launching angle and the critical force. These adjustments were kept constant within each data set.

Only a handful of data are shown in this publication. Altogether 25 sets of data were collected. Fig. 10 and Fig. 11 show the comparison for a fixed clamping angle ($\theta = -0.0225$ and -0.025 radians, respectively) as the inverse pendulum height is varied. The theoreti-

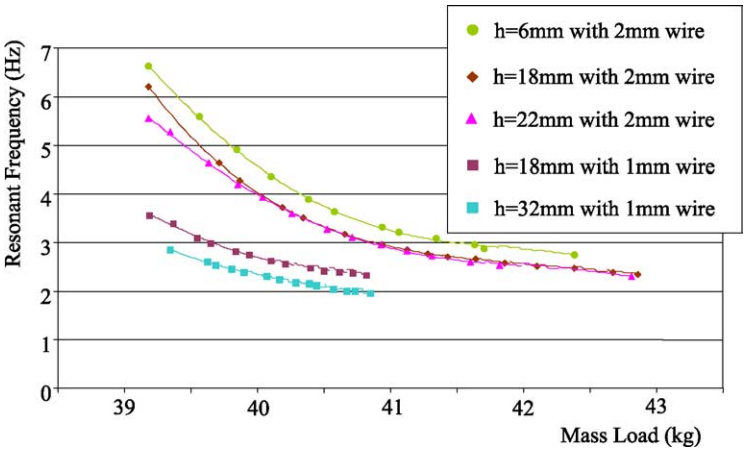

Fig. 9. Plot of the resonant frequency as a function of mass in the Euler stage with different values of the inverse pendulum height h. The distinct different operating ranges in mass load between the different sized wires clearly suggests the system with the 1 mm wire is softer.

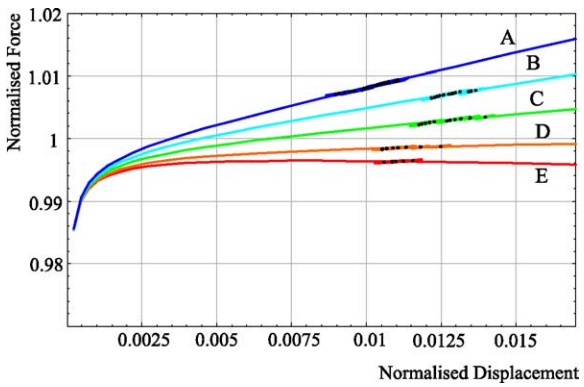

Fig. 10. The force–displacement curves for experimental launch angle $\theta = -0.0225$ radians (adjusted to -0.00070 rads), (A) $h = 45$ mm, (B) $h = 55$ mm, (C) $h = 65$ mm, (D) $h = 75$ mm, and (E) $h = 81$ mm.

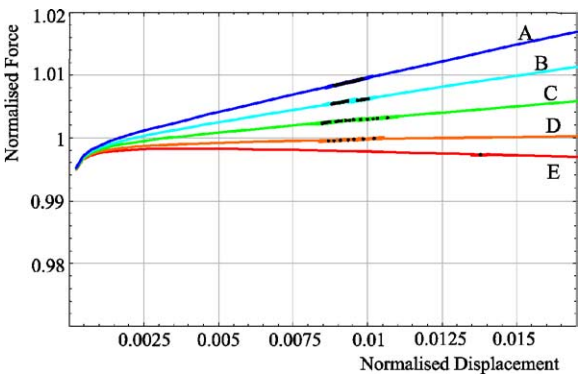

Fig. 11. The force–displacement curves for experimental launch angle $\theta = -0.025$ radians (adjusted to -0.00023 rads), (A) $h = 45$ mm, (B) $h = 55$ mm, (C) $h = 65$ mm, (D) $h = 75$ mm, and (E) $h = 81$ mm.

cal values of θ used to produce the curves are given in the captions. Adjustments of the critical force to match experimental data were minimal, with a maximum of 1% variation. The analysis of these plots suggests that the performance behaves as expected although large deviations are seen between the theoretical and experimental launching angles. These and similar plots show a trend corresponding to the upper part of Fig. 2. As θ becomes more negative in Fig. 2, the curves approach the desirable dark curve which has an almost constant spring coefficient. As θ decreases further, regions of instability represented by negative gradients start to appear. The force–displacement curves fitting the experimental data show this trend.

The launching angle discrepancies between theoretical and experimental results were mainly due to non-ideal conditions in the experimental setup. Creep and the inelastic performance in the springs due do continual use played a major part. The wedges were difficult to adjust as they were able to slip with respect to one another changing the lengths of the Euler springs. Also, there was error in defining the exact clamping point as the wedges have finite roundness on the edges.

Fig. 12 shows four transfer functions illustrating the progressive improvements made on the Euler vertical stage [17]. The first transfer function (a) is obtained using an older design [10]. Transfer function (b) is ob-

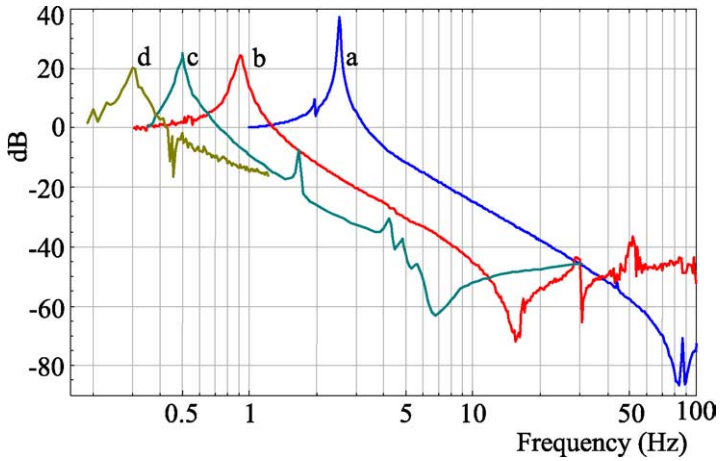

Fig. 12. The progressive improvement in the transfer functions: (a) using a previous Euler stage design with a resonant frequency of 2.5 Hz, (b) the transfer function of the launching angle $\theta = 0.0225$ rads at $h = 75$ mm during the experimental investigations with a resonant peak at 0.92 Hz, (c) obtained from implementing improved methods into system achieving a resonant frequency of 0.50 Hz, and (d) with the latest stage design using maraging steel Euler springs with a resonant frequency of 0.3 Hz.

tained from the configuration having a launch angle of -0.0225 rads with $h = 75$ mm achieving a resonant frequency of 0.92 Hz. An even lower resonant frequency of 0.62 Hz is achieved having a spring coefficient of just over 650 N/m using the configuration of $\theta = -0.025$ rads at the inverse pendulum height of 81 mm.

Following this, several design changes were made. A different spring material was trialled: the AISI 301 having higher yield strength and a lower creep rate. Secondly, a new design which allowed for better clamping and finer launching angle adjustments was installed. A new wire holder suitable for holding 0.5 mm diameter suspension wires was also constructed to further soften the system. The resulting transfer function is shown in Fig. 12(c) achieving a resonant frequency of 0.50 Hz. Additional modes were introduced by the modified stage appearing between the resonant peaks of 0.5 Hz to about 6 Hz.

In an attempt to eliminate some of the problems discussed above (namely clamping conditions and creep), a new and improved vertical stage configuration was designed [17]. The Euler springs were relocated so that their vertical displacements were collinear with the suspension points. To further reduce creep, the spring steel was replaced with maraging steel [21]. A creep rate of less than 1 μm/day for a 40 kg load was recorded. The transfer function of Fig. 12(d) was taken using a test mass of approximately 80 kg with an Euler spring length of 175 mm with thickness 0.8 mm. A resonant frequency of 0.3 Hz was obtained for zero launching angle.

While obtaining transfer function (c) a Q-factor of 35 was observed at 0.62 Hz. The Q-factor decreases with frequency squared as mentioned previously. This suggests that it may be possible to obtain a resonant frequency of order 0.1 Hz before the losses dominate the system.

5. Discussion and conclusion

The implementation of inverse pendulums into Euler spring vibration isolators has reduced the resonant frequency of the vertical Euler stage to below 1 Hz. Non-linearities can be reduced by adjusting the spring launching angles. While adjustment of the launching angle is advantageous, it is difficult to reproduce theoretical predictions due to imperfections in the system. Issues concerning the stability of the Euler stage have been identified. A resonant frequency of 0.3 Hz was achieved for a single vertical isolation stage. This is about 100 times softer than a comparable cantilever blade spring.

All the transfer functions shown in Fig. 12 show classic centre of percussion effects [10,19,20]. These

effects can be tuned out by adjusting the mass distribution of the rotational arm. This will be necessary to maintain good isolation at high frequency. Theoretical and experimental work on the Euler stage centre of percussion tuning will be presented in a future publication.

Acknowledgements

This work is supported by the Australian Research Council, and is part of the Australian Centre for Interferometric Gravitational Astronomy. The authors wish to thank the workshop technicians Peter Hay, Ken Field, and Michael Kemp. We would also like to acknowledge John Jacob for his involvement.

References

[1] L. Ju, et al., Rev. Sci. Instrum. 65 (1994) 6482.
[2] D.G. Blair, et al., Meas. Sci. Technol. 2 (1991) 846.
[3] G. Losurdo, et al., Rev. Sci. Instrum. 70 (1999) 2507.
[4] G. Ballardin, et al., Rev. Sci. Instrum. 72 (2001) 3643.
[5] M.V. Plissi, et al., Rev. Sci. Instrum. 71 (2000) 2539.
[6] R. Takahashi, et al., Class. Quantum Grav. 19 (2002) 1599.
[7] R. Takahashi, et al., Rev. Sci. Instrum. 73 (2002) 2428.
[8] S. Marka, et al., Class. Quantum Grav. 19 (2002) 1605.
[9] R. Abbott, et al., Class. Quantum Grav. 19 (2002) 1591.
[10] J. Winterflood, et al., Phys. Lett. A 300 (2002) 122.
[11] J. Winterflood, High performance vibration isolation for gravitational wave detection, http://www.physics.uwa.edu.au/pub/Thesis/PhD, 2001, p. 7.
[12] J. Winterflood, et al., Phys. Lett. A 300 (2002) 131.
[13] T. Barber et al., High performance vibration isolation for gravitational wave detection, 2004, in press.
[14] J. Winterflood, et al., Phys. Lett. A 243 (1998) 1.
[15] A. Bertolini, et al., Nucl. Instrum. Methods Phys. Res. A 435 (1999) 475.
[16] G. Cella, et al., Nucl. Instrum. Methods Phys. Res. A 487 (2001) 652.
[17] E.J. Chin, et al., Class. Quantum Grav. 21 (2004) 959.
[18] W.D. Weinstein, Machine Design 37 (1965) 150.
[19] J. Liu, et al., Phys. Lett. A 228 (1997) 243.
[20] F. Garoi, et al., Rev. Sci. Instrum. 74 (2003) 3487.
[21] M. Beccaria, et al., Nucl. Instrum. Methods Phys. Res. A 404 (1997) 455.